Wake effect on a uniform flow behind wind-turbine model

Okulov, Valery; Naumov, I. V.; Mikkelsen, Robert Flemming; Sørensen, Jens Nørkær

Published in:
Journal of Physics: Conference Series (Online)

Link to article, DOI:
10.1088/1742-6596/625/1/012011

Publication date:
2015

Document Version
Publisher's PDF, also known as Version of record

Wake effect on a uniform flow behind wind-turbine model

2015 J. Phys.: Conf. Ser. 625 012011

(http://iopscience.iop.org/1742-6596/625/1/012011)

Wake effect on a uniform flow behind wind-turbine model

V L Okulov [1,2] I V Naumov[2], R F Mikkelsen[1], and J N Sørensen[1]

[1]Department of Wind Energy, Technical University of Denmark, 2800 Lyngby, Denmark
[2] Institute of Thermophysics, SB RAS, Novosibirsk 630090, Russia

E-mail: okulov@dtu.dk

Abstract. LDA experiments were carried out to study the development of mean velocity profiles of the very far wake behind a wind turbine model in a water flume. The model of the rotor is placed in a middle of the flume. The initial flume flow is subjected to a very low turbulence level, limiting the influence of external disturbances on the development of the inherent wake instability. The rotor is three-bladed and designed using Glauert's optimum theory at a tip speed ratio λ =5 with a constant of the lift coefficient along the span, C_L= 0.8. The wake development has been studied in the range of tip speed ratios from 3 to 9, and at different cross-sections from 10 to 100 rotor radii downstream from the rotor.

By using regression techniques to fit the velocity profiles it was possible to obtain accurate velocity deficits and estimate length scales of the wake attenuation. The data are compared with different analytical models for wind turbine wakes.

1. Introduction

Due to the fast growth in the number of wind farms around the world extensive investigations have been carried out during the past two decades to better understand and predict wake flows behind wind turbines. The velocity deficit and turbulence levels in the wakes are parameters that define the available power and structural stability of wind turbines located downwind of other turbines in the farms. In spite of the extensive investigations, the prediction of wake evolution and decay are still open questions [1].

Various analytical approaches have been applied to describe the wind-turbine wakes, but a general model for the wake based on a common solution to predict the wake behavior under different wind conditions has still not been found. Among them, so-called kinematic models were obtained from experimental and theoretical works [2]. The kinematic models are based on self-similar velocity deficit profiles obtained from global momentum conservation, using as input the thrust coefficient of the wind turbine. One of the pioneering kinematic models of the far wake behind wind turbines assumed a top-hat shape for the velocity deficit [3]. Hereinafter we will refer all models to the first letter of the author's name, as such the J-model for the model of Jensen [3]. Lately, yet an analytical wake model was proposed and validated to predict the wind velocity distribution in the wake [4]. This BP-model is derived by applying conservation of mass and momentum and assuming a Gaussian distribution for the velocity deficit in the wake.

Out of these considerations of the wind-turbine wakes, George [5] proposed a new methodology for the far wake behind axisymmetric bluff bodies. This G-model of wake was called "equilibrium similarity" analysis when the axisymmetric profiles at a self-similarity state wake asymptotically

attenuates at the same rate independent of the way it is generated. He also argued that the Reynolds number is the main factor in determining the rate of the axisymmetric wake. This theory was successfully confirmed by comparison to experimental data for the axisymmetric wake behind a streamline disk [6-8] in a wind tunnel. Based on these studies, the two different rates for the G-model were confirmed for very high and low local Reynolds numbers in the disk wake.

The current paper investigates the far wake of a three-bladed HAWT rotor, with a blade design based on the Glauert optimum rotor [9]. The purpose of the present investigation is to determine the wake development and decay properties observed in the far wake behind the rotor to compare it with the wake behind disk to estimate a possibility of the G-model for the wind-turbine wake. Compared to the flow around a bluff body, it is, however, rather difficult to discriminate between the various decay properties of the far field behind a rotor. A difference in the strength of the wake deficit behind a wind turbine and a disk of the same radius is not fully understood. Indeed the various types of the decay properties for both disk and rotor wakes may be of quite different nature. Moreover some difference may also exist in the wake development for different operating regimes of the wind turbine (with different thrust coefficient or tip speed ratio). The last question did not else clear even for the basic J- and BP models mentioned above [4].

Therefore, in the present study, a special attention has been paid to detect and categorize the various types of wake development behind the wind turbine under the different operation in a range of the tip speed ratio (TSR) from 2 to 10. The LDA-measurements at different cross-sections of the far wake up to 50 rotor diameters downstream from the rotor are accomplished by a comparison with the three basic analytical models mentioned above.

2. Experimental Method

The experiment is carried out in a water flume of length 35m, 3m width and an operative height of 0.9m. The 3m wide test section is fitted with transparent walls at a distance of 20 m from the channel inlet. The free flow speed in the flume was $U = 0.64$m/s. In order to filter out disturbances, the water was led through an inlet equipped with honeycomb. Prior to the experiment, the velocity profiles were measured at various positions in the flume in order to determine a cross section with as constant velocity as possible (figure 1). The velocity profile variation of the incoming water flow is less than 1% during all experiments, measured with LDA and an independent OTT Z400 velocimeter. This diagram indicates that the velocity profile is constant 0.25m from the edges and across the flume in the region 0.25-0.65m above the bottom with a minimal oscillation of the free flow (figure 2). Based on the measured velocity the rotor axis was positioned at a height of 0.5m from the channel bottom and 0.7m away from the flume walls [9, 11].

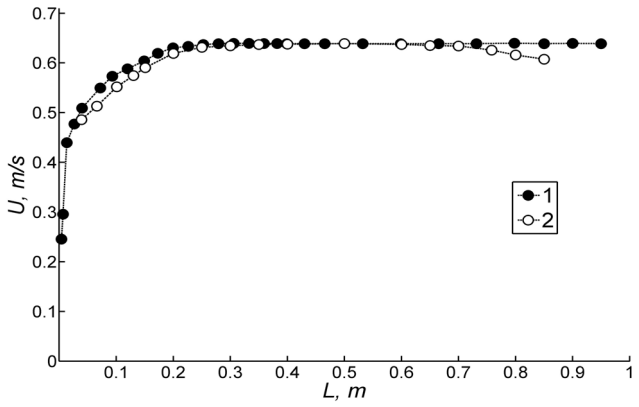

Figure 1. Free stream conditions (mean velocity) in the rotor cross section: average velocity profiles: 1 – from wall to rotor, 2 – from flume bottom to rotor.

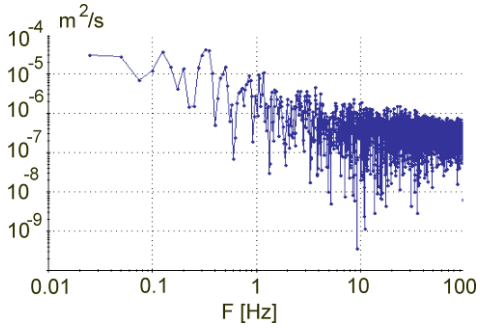

Figure 2. Spectrum of the free flow oscillations in the rotor area.

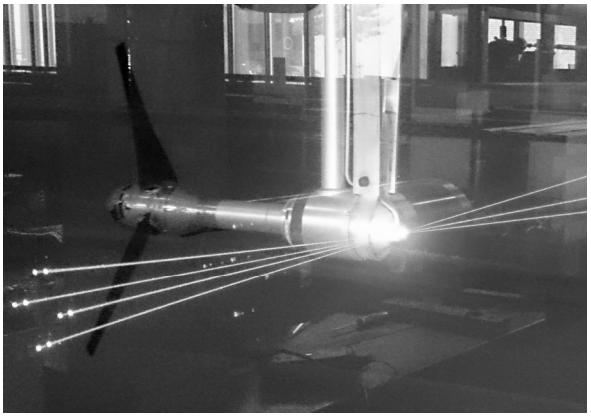

Figure 3. Photo of the model rotor and the LDA measurements.

The three-bladed model rotor has a diameter D = 0.376m with blades of length 0.159m, consisting of SD7003 airfoil sections (figure 3). The shape and pitch setting of the blade were calculated using the theory of Glauert [10] for optimum operating conditions at a tip speed ratio $\lambda = 5$, where $\lambda = \Omega R/U$, and Ω is angular speed of the rotor. The Reynolds numbers based on rotor diameter and free stream was varied in the range 140.000 <*Re*< 240.000. As working fluid, tap water at a temperature of 20ºC was used.

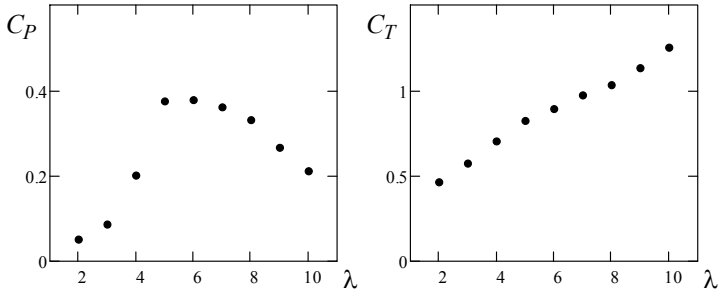

Figure 4. Measured power and trust coefficients as functions of tip speed ratio [9].

The rotor was driven by a JVL Industri Elektronik MAC400 servo motor which was operated at a constant rotational speed within 2% accuracy. The angle of attack of the blade was fixed for each test case. The torque of the motor was transferred to the rotor axis via a rigid gear transmission. The power (C_P) and thrust (C_T) coefficients were measured for different tip speed ratios (figure 4 and table 1).

Table 1. Power and thrust coefficients as function of tip speed ratio

λ	C_P	C_T
2	0.05	0.46
5	0.37	0.83
8	0.33	1.01
10	0.21	1.25

The flow downstream of the rotor develops into two different structures of the near and far wakes. The near wake defines as well-defined 3D structure consisting of slender vortices in which the helical tip vortices are undoubtedly visualized by fluorescence dye (figure 5) [12-13].

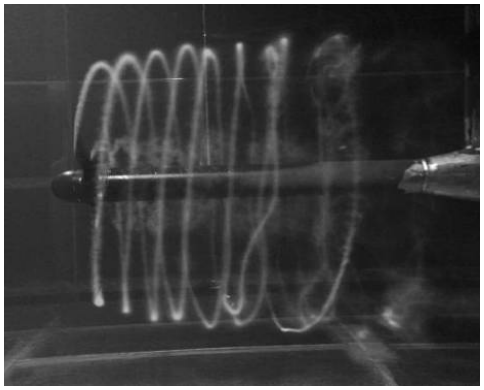

Figure 5. Dye visualization of the 3-D vortex structure in the near wake.

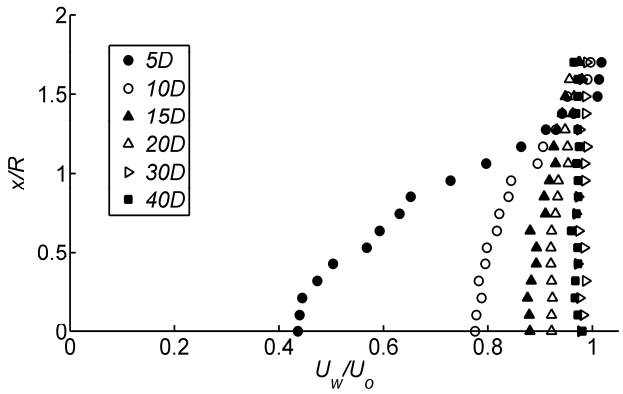

Figure 6. LDA-test of the far wake deficit of wind turbine with an optimal value of the tip speed ratio ($\lambda = 5$).

The visualizations are however not useable to detect the flow structures in the far wake of the rotor because the initial helical structure disappears due to mixing when the vortices become unstable and starts pairing up [9, 13]. A more accurate recognition of the flow structures was obtained using LDA (figure 6). To obtain more information about the far wake development, the flow velocities were measured with high temporal accuracy using LDA. These measurements were carried out through all wake area with stream-wise steps of 10*R* and at different radial positions from the rotor axis with the step of 0.1*R*. In each point the local axial velocity history was obtained using a Dantec 2-D Fiber flow LDA, based on a 1W Argon laser with a differential optical configuration with a frequency shift of 40 MHz. The diameter of the optical gauge is 112mm and the focal length is 600mm with a beam diameter of 1.35mm. The wavelength of the laser beam is 514.5 nm (green light). The size of the probing optical field was $0.12\times0.12\times1.52\text{mm}^3$. The signal from the light-scattering particles is collected and processed by a Burst Specter Analyzer (BSA57N2 commercial signal processor) to detect the characteristic frequencies in the flow. Each time history was recorded in a period of 60s, corresponding to about 20 - 50 rotor rotation.

3. The analytical models of the far wake development

Based on the three basic models mentioned in the Introduction we will write the following expression for the maximal values of the velocity deficit

$$\frac{\Delta U}{U_0} = \frac{\max\left(U_0 - U_w\right)}{U_0}, \tag{1}$$

where U_0 is the free wind speed; U_w is velocity in the wake cross-sections and ΔU is the maximal velocity deficit. In the axisymmetric wake the maximum of the deficit lies on the rotor axis.

For the deficit maximum of (1) the J-model [3] can be expressed by a simple formula:

$$C_J\left(x\right) \equiv \frac{\Delta U}{U_0} = \frac{1-\sqrt{1-C_T}}{\left(1-\frac{2k_w x}{D}\right)^2}, \tag{2}$$

where C_T is the thrust coefficient from the table 1; k_w is the rate of the wake expansion and D is the rotor diameter. Jensen [3] assumed a top-hat shape for the velocity deficit and considered a constant

value of the wake expansion ($k_w = 0.1$). However, $k_w = 0.075$ is the value usual used in literature [14].

The BP-model [4] is proposed to predict the maximum deficit of the streamwise velocity in the wake by the formula:

$$C_{BP}(x) \equiv \frac{\Delta U}{U_0} = 1 - \sqrt{1 - \frac{C_T}{8\left(\frac{k^* x}{D} - 0.2\sqrt{\beta}\right)^2}}, \tag{3}$$

where k^* represents the wake growth rate and β is obtained by the equation

$$\beta = \frac{1 + \sqrt{1 - C_T}}{2\sqrt{1 - C_T}}. \tag{4}$$

The author of the BP-model [4] assumed a Gaussian shape for the velocity deficit

$$\frac{U_0 - U_w}{U_0} = C_{BP}(x) \exp\left(-\frac{r^2}{2\sigma^2}\right), \tag{5}$$

where r is radial distance from the rotor axis and $\sigma = k^* x + \varepsilon$ is the standard deviation of the Gaussian-like velocity deficit profiles (5) at each x. The authors of [4] have considered a constant value of the wake growth rate ($k^*/D = 0.023$ and 0.031) in which the small deviations depend from operating regimes with different values of the thrust coefficient. However, $k^*/D = 0.015$ is best to fit the wake on the wind turbine optimum for our experience.

The G-model [5] was originally proposed to predict the wake decay behind a solid disk. Using similarity theory the maximum deficit of the streamwise velocity in the wake for high-Reynolds-number is described by the formula [8]:

$$C_G(x) \equiv \frac{\Delta U}{U_0} = h(x - x_0)^{-2/3}, \tag{6}$$

where x_0 is a virtual origin and the parameters a and x_0 depend on the type of the bluff body generating the wake, which, however, must keep the power $-2/3$ for any wake generators. Downstream evolution of the centreline velocity deficit behind his disk conditions was found excellent for the constants $h = 0.77$ and $x_0 = -2.4$.

Instead of the Gaussian shape for the velocity deficit (5), the G-model [6] assumed to fit it by a curve of the form

$$\frac{U_0 - U_w}{U_0} = C_G(x)\left(1 + a\eta^2 + b\eta^4\right)\exp\left(-c\eta^2 - d\eta^4\right), \tag{7}$$

where $a = 0.049$; $b = 0.128$; $c = 0.345$; $d = 0.134$ and $\eta = r/L$ is a non-dimension radial distance scaling by position where the maximum of the velocity deficit reduced to a half value $\frac{1}{2}\Delta U$

4. Development of the far wake behind a 3-blade rotor

Initially we try to separate the zones of the near and the far wake. The dye tracers in figure 5 give a good impression of the structure of the tip vortices in the near wake [9, 13], which shows the tip vortices as continuous curves giving a nearly perfect helical shape with a slight expansion. These photos also indicate an onset of initial disturbances for all operating regimes in the early development of the wake (approximately 2*D* downstream) as well as the initial point of onset of the transitional regime to far wake. This happens approximately 4*D* downstream from the rotor, where a full mixing of the dye tracers is seen to take place. The mixing connects with the wake instability and may be explained as a transition from the onset of initial disturbances to a fully developed far wake at 6*D* distance behind rotor. Due to the mixing in the far wake, the visualizations gave no information about the far wake behavior. As a consequence, to achieve a more accurate picture of the wake development, the visualizations were supplemented by LDA measurements in a number of points downstream of the rotor (see figure 6). Analyzing the LDA-spectra of the axial velocity in the rotor wake also confirmed the existence of two different zones of the wake with different main frequencies [9]. In the tested region the main flow oscillations have been determined to be associated with the blade and rotor frequencies in the near wake up to 6*D* distance behind rotor. Only a single dominating oscillation at a very low frequency has been indicated in far wake area after a distance of 6*D*.

Afterward we have analyzed the various LDA-profiles of the axial velocity in different cross-sections of the far wake at distances from 5*D* to 40*D* behind the rotor (see figure 6) and for the rotor operating under different tip speed ratios (see table 1). The self-similar velocity-deficit profiles at different downwind wake distances are shown in figure 7 for the optimum operating regime with $\lambda = 5$ and in figure 8 the different rotor operations. At each x the wake's half-width defined as

$$\left.\frac{U_0 - U_w}{U_0}\right|_{r=\frac{1}{2}L} = \frac{1}{2}\frac{\Delta U}{U_0}, \tag{8}$$

Figures 7 and 8 show that all wake profiles scaled by (8) approximately coinside with the Gaussian curve (5) from [4] except at the edge of the wake but approximation by the curve (7) introduced in [7] is excellent for fitting this data. It means that the velocity deficit profile can be assumed to be self-similar in far wakes. For $\lambda = 2$ (figure 8) the velocity profile is Gaussian instead of the one proposed by G-model. This is most likely explained by the lack of axial symmetry of the wake at very slow rotation of the three blades.

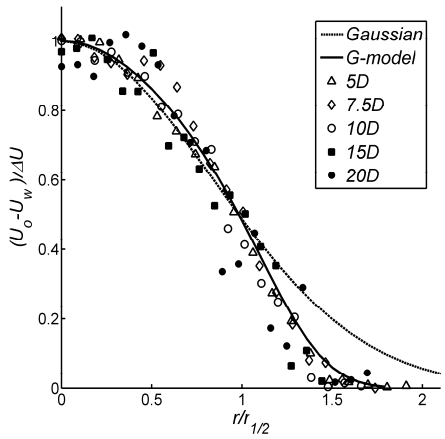

Figure 7. The self-similar behavior of the velocity deficit profiles in the wake on the optimum $\lambda = 5$.

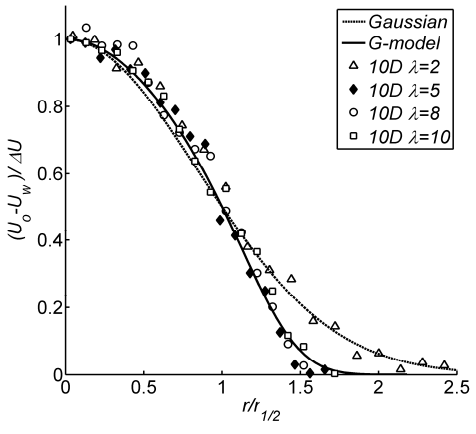

Figure 8. The self-similar behavior of the velocity deficit profiles in the wakes with $\lambda = 2, 5, 8, 10$.

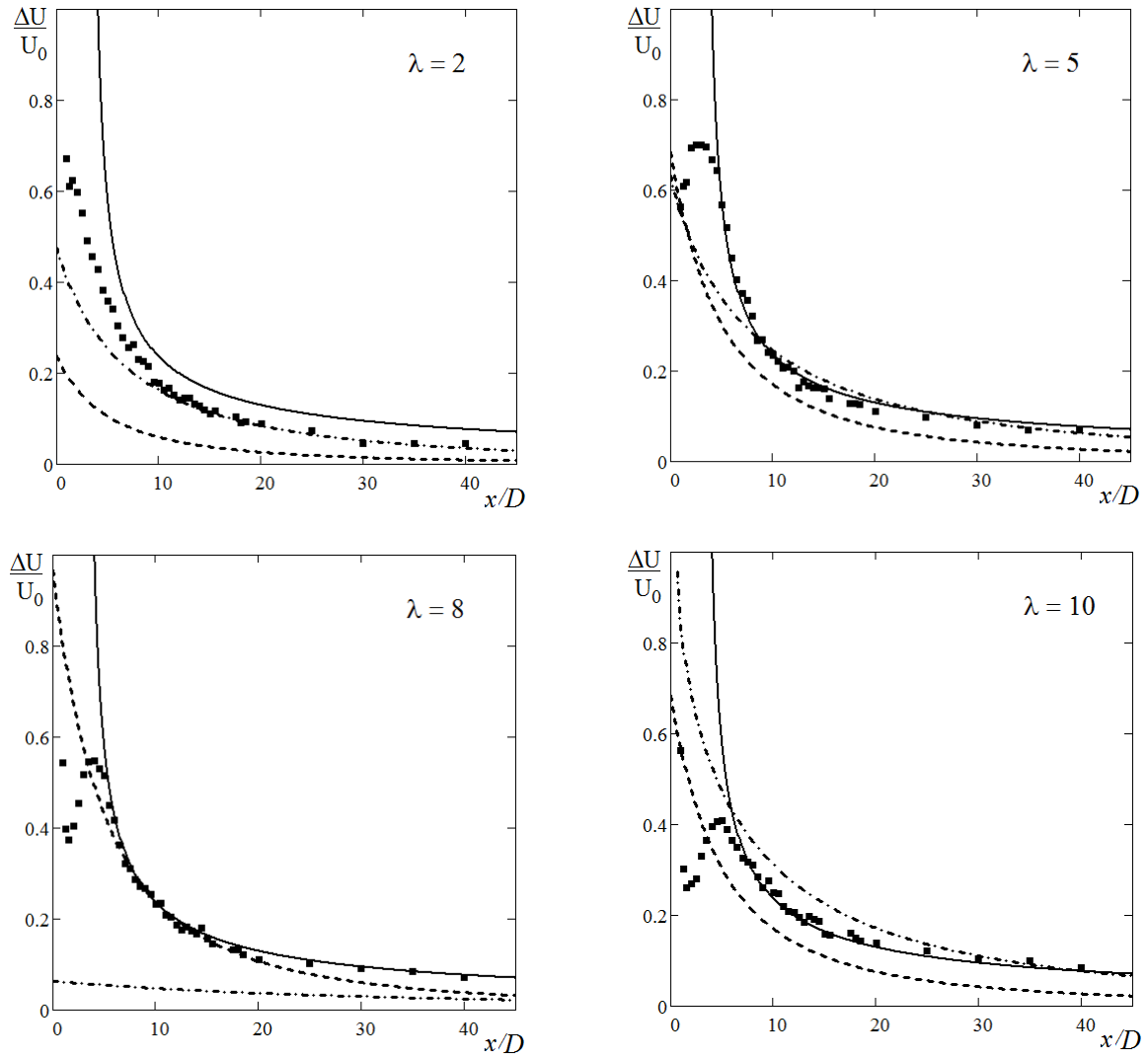

Figure 9. Downstream evolution of the maximal velocity deficit for different λ = 2, 5, 8, 10: Points – experiment; solid lines - C_G ; dashed lines - C_J ; dot-dashed lines - C_{BP}

The streamwise variation of the maximum velocity deficit in the rotor wake under the different tip speed ratios is shown in figure 9. It is clear that this value decreases monotonically and in a smooth manner for the different rotor operations. The solid line shows the high-Reynolds-number equilibrium similarity solution discussed below in equation (6) which was proposed in [5]. For cases of the wake evolution, the same constants, $h = 0.85$ and $x_0 = 3.2$, in (6) was used for the solid curve fitting. The first plot for the very low tip speed ratio (λ = 2) gives different values of the experimental data with (6), but next ones indicate the same behaviour with (6) which does not depend from the rotor thrust for all values of λ > 2. The first case has a different value only because the very slow rotation of the three blades could not form a symmetrical far wake.

The dashed and dot-dashed lines show the curves represented by (2) and (3) of the J- and BP-models. Unfortunately these models disagree with the experimental data.

5. Conclusions

The flow behind the model of a horizontal axis wind turbine rotor was investigated experimentally in a water flume. The initial flume flow was subject to a very low turbulence level and a uniform velocity profile, limiting the influence of external disturbances on the development of the far wake. The wake

has been studied at different cross-sections from the near wake up to 40 rotor diameters downstream from the rotor. In the result of the present investigation the far wake development and decay properties have been determined and observed behind the rotor under different operating regimes for λ = 2-10. The data was used to compare the different wake models by Jensen [3] (J-model); Bastankhan & Porte-Agel [4] (BP-model) and the disk wake model by George [5] (G-model) which was extended to the rotor wake here.

The comparison with our high-resolution LDA measurements shows that the velocity profiles obtained with the disk-wake G-model after an expansion to the rotor wake are in acceptable agreement with the experimental data. By contrast, the J- and BP models generally underestimate the velocity deficit at the centerline of the wake. Our results also reveal that the G-model is consistent and acceptably accurate also in terms of the power estimation for the long distance of the wake development whereas J- and BP-models are less accurate.

6. Acknowledgments

The present work has been carried out with the support of the Danish Council for Strategic Research for the project COMWIND (grant 2104-09-067216/DSF) and the Russian Science Foundation (grant 14-19-00487). The authors also express their thanks to K.E. Meyer for useful discussions and help in calibration of LDA equipment during experiments.

References

[1] Vermeer L, Sørensen J, Crespo A. Wind turbine wake aerodynamics. *Prog Aerosp Sci* 2003; 39: 467-510.
[2] Lissaman PBS. Energy effectiveness of arbitrary arrays of wind turbines. In: *AIAA Paper* 79-0114, 1979. p. 1–7.
[3] Jensen N. A note on wind turbine interaction. Technical report Ris-M-2411. Roskilde, Denmark: Risø National Laboratory; 1983.
[4] Bastankhan M, Porte-Agel F. A new analytical model for wind turbine wakes. *Renewable Energy* 2014; 70: 116-123.
[5] George WK. The self-preservation of turbulent flows and its relation to initial conditions and coherent structures. *Advances in Turbulence*, 1989: p. 39-73.
[6] Johansson PBV, George WK, Gourlay MJ. Equilibrium similarity, effects of initial conditions and local Reynolds number on the axisymmetric wake. *Physics of Fluids*, 2003; 15(3): 603-617.
[7] Johansson PBV. The axisymmetric turbulent wake. PhD thesis of Department of Thermo and Fluid Dynamics, Chalmers University of Technology, 2002.
[8] Johansson PBV, George WK. The far downstream evolution of the high-Reynolds-number axisymmetric wake behind a disk. Part 1. Single-point statistics. *J. Fluid Mech.* 2006; 555: 363-386.
[9] Okulov VL, Naumov IV, Mikkelsen RF, Kabardin IK, Sørensen JN. A regular Strouhal number for large-scale instability in the far wake of a rotor. *J. Fluid Mech.* 2014; 747: 369-380.
[10] Glauert H 1935 Airplane propellers *Aerodynamic Theory* ed. W.F.Durand (Berlin: Springer) **IV**
[11] Naumov IV, Rahmanov VV, Okulov VL, Velte CM, Meyer KE, Mikkelsen RF 2012 Flow diagnostics downstream of a tribladed rotor model. *Thermophysics & Aeromechanics* **19(2)** 253-263
[12] Okulov VL, Naumov IV, Mikkelsen RF, Kabardin IK, Sørensen JN. Experimental investigation of the wake behind a model of wind turbine in a water flume. *Journal of Physics: Conference Series* 2014; 555: 012080. DOI: 10.1088/1742-6596/555/1/012080
[13] Naumov IV, Mikkelsen RF, Okulov VL, Sørensen JN. PIV and LDA measurements of the wake behind a wind turbine model. *Journal of Physics: Conference Series* 2014, vol. 524, 012168; doi:10.1088/1742-6596/524/1/012168
[14] Barthelmie RJ, Folkerts L, Larsen GC, Rados K, Pryor SC, Frandsen ST, et al. Comparison of wake model simulations with offshore wind turbine wake profiles measured by sodar. *J Atmospheric Ocean Technol* 2005; 23: 881-901.